Atmospheric
Chemistry
and Physics

Phase state of secondary organic aerosol in chamber photo-oxidation of mixed precursors

Yu Wang[1], Aristeidis Voliotis[1], Yunqi Shao[1], Taomou Zong[2], Xiangxinyue Meng[2], Mao Du[1], Dawei Hu[1], Ying Chen[3,a], Zhijun Wu[2,4,5], M. Rami Alfarra[1,6,7], and Gordon McFiggans[1]

[1]Centre for Atmospheric Science, Department of Earth and Environmental Sciences,
The University of Manchester, Manchester M13 9PL, UK
[2]State Key Joint Laboratory of Environmental Simulation and Pollution Control, International Joint Laboratory for Regional Pollution Control, Ministry of Education (IJRC), College of Environmental Sciences and Engineering,
Peking University, Beijing 100871, China
[3]Lancaster Environment Centre, Lancaster University, Lancaster LA1 4YQ, UK
[4]International Joint Laboratory for Regional Pollution Control, 52425 Jülich, Germany, and Beijing 100871, China
[5]Collaborative Innovation Center of Atmospheric Environment and Equipment Technology,
Nanjing University of Information Science and Technology, Nanjing 210044, China
[6]National Centre for Atmospheric Science, School of Earth and Environmental Sciences,
The University of Manchester, Manchester M13 9PL, UK
[7]Qatar Environment and Energy Research Institute, Hamad Bin Khalifa University, Doha, Qatar
[a]currently at: Exeter Climate Systems, University of Exeter, Exeter EX4 4QE, UK

Correspondence: Gordon McFiggans (g.mcfiggans@manchester.ac.uk)

Abstract. The phase behaviour of aerosol particles plays a profound role in atmospheric physicochemical processes, influencing their physical and optical properties and further impacting climate and air quality. However, understanding of the aerosol phase state is still incomplete, especially that of multicomponent particles which contain inorganic compounds and secondary organic aerosol (SOA) from mixed volatile organic compound (VOC) precursors. We report measurements conducted in the Manchester Aerosol Chamber (MAC) to investigate the aerosol rebounding tendency, measured as the bounce fraction, as a surrogate of the aerosol phase state during SOA formation from photo-oxidation of biogenic (α-pinene and isoprene) and anthropogenic (o-cresol) VOCs and their binary mixtures on deliquescent ammonium sulfate seed.

Aerosol phase state is dependent on relative humidity (RH) and chemical composition (key factors determining aerosol water uptake). Liquid (bounce fraction; BF < 0.2) at RH > 80 % and nonliquid behaviour (BF > 0.8) at RH < 30 % were observed, with a liquid-to-nonliquid tran-

sition with decreasing RH between 30 % and 80 %. This RH-dependent phase behaviour ($RH_{BF=0.2, 0.5, 0.8}$) increased towards a maximum, with an increasing organic–inorganic mass ratio ($MR_{org/inorg}$) during SOA formation evolution in all investigated VOC systems. With the use of comparable initial ammonium sulfate seed concentration, the SOA production rate of the VOC systems determines the $MR_{org/inorg}$ and, consequently, the change in the phase behaviour. Although less important than RH and $MR_{org/inorg}$, the SOA composition plays a second-order role, with differences in the liquid-to-nonliquid transition at moderate $MR_{org/inorg}$ of ~ 1 observed between biogenic-only (anthropogenic-free) and anthropogenic-containing VOC systems. Considering the combining role of the RH and chemical composition in aerosol phase state, the BF decreased monotonically with increasing hygroscopic growth factor (GF), and the BF was ~ 0 when GF was larger than 1.15. The real atmospheric consequences of our results are that any processes changing ambient RH or $MR_{org/inorg}$ (aerosol liquid water) will influence their phase state. Where abundant anthropogenic VOCs

contribute to SOA, compositional changes in SOA may influence phase behaviour at moderate organic mass fraction (~ 50 %) compared with purely biogenic SOA. Further studies are needed on more complex and realistic atmospheric mixtures.

---

1   Introduction

Aerosol particles are ubiquitous in the atmosphere and can act as reaction vessels where physicochemical processes occur. As one of the key physical properties of aerosol particles, the aerosol phase state can significantly impact those physicochemical processes (Martin, 2000). Following the pioneering work of Virtanen et al. (2010), there has recently been a considerable effort to resolve the influences of aerosol phase state from a number of perspectives, mainly relating to the retardation of diffusion or mobile components including water. The viscous solid particles have potential impacts on physicochemical processes, such as constraining gas particle partitioning of semi-volatile organic species (Vaden et al., 2011; Shiraiwa et al., 2011; Shiraiwa and Seinfeld, 2012; Zaveri et al., 2014; Renbaum-Wolff et al., 2013), heterogeneous reactions, or liquid-phase reactions (Shiraiwa et al., 2011; Koop et al., 2011; Kuwata and Martin, 2012; Zhang et al., 2018; Martin, 2000). These processes affect secondary organic and inorganic particulate matter formation in the atmosphere, further impacting their optical properties and air quality. Moreover, the ice nucleation abilities in the upper tropospheric conditions and cloud condensation nuclei activation of aerosol particles are affected by the phase behaviour (Pöschl, 2011; Murray et al., 2010; Murray, 2008; Reid et al., 2018; Shiraiwa et al., 2017; Ignatius et al., 2016; Slade et al., 2017), further impacting cloud formation and regional climate. Better understanding the phase behaviour of atmospheric particles is important for understanding physicochemical processes in the atmosphere and aerosol–cloud interactions.

The particle rebounding property has been widely used to study the phase behaviour of aerosol particles (Dahneke, 1971; Stein et al., 1994). In a real atmosphere, the phase behaviour of aerosol particles varied significantly under various environments, depending on the ambient relative humidity (RH) and aerosol chemical composition. For example, background atmospheric particles in the tropical rainforest over central Amazonia, mainly composed of isoprene-derived secondary organic aerosol (SOA), were initially liquid for ambient RH > 80 % and temperatures of 23–27 °C (Bateman et al., 2015b). In contrast, when the measurement site was influenced by anthropogenic air mass from urban pollution and biomass burning, the nonliquid PM fraction increased to 60 % at 95 % RH (Bateman et al., 2017). However, in the boreal forest of northern Finland, atmospheric particles (mainly monoterpene-derived SOA) showed an amorphous, solid-like phase state (Virtanen et al., 2010). An enhanced fraction of particulate sulfate can lead to loss of particle bounce, and atmospheric particles with high fraction of inorganic compounds showed a liquid-like phase state under moderate and high ambient RH, e.g. an urban area (Liu et al., 2017), a subtropical coastal megacity (Liu et al., 2019), a southeastern USA rural site (Pajunoja et al., 2016), and a northeastern near-forest area (Slade et al., 2019)). When the terpene-dominant SOA increased during nighttime (Slade et al., 2019) or ambient RH dropped under 60 % (Liu et al., 2017), the nonliquid PM increased.

Consistent with the main findings in the field studies, the particle bounce of pure SOA from the oxidation of representative biogenic or anthropogenic VOC (volatile organic compound; e.g. isoprene, α-pinene, and toluene) decreased with elevated RH and varied with SOA composition (Bateman et al., 2015a; Saukko et al., 2012). The discrepancy between the Bateman et al. (2015a) and Saukko et al. (2012) was the RH at which aerosol particles fully adhered to the substrate (with < 20 % aerosol particles rebounding; referred as the adhesion RH). In a well-calibrated rebounding impactor system, the rebound or adhering behaviour is highly related to the aerosol phase state, which is determined by material softening. Bateman et al. (2015a) found the complete adhesion RH for the isoprene SOA, α-pinene SOA, 2 : 1 isoprene/α-pinene mixture, and toluene SOA was > 65 %, > 95 %, > 80 %, and > 80 %. However, Saukko et al. (2012) observed that SOA from isoprene and α-pinene oxidation, do not fully adhere to the substrate RH of up to 90 %. This discrepancy might due to the slightly different instrumentation design (pressure drop in Saukko et al., 2012, vs. atmospheric pressure in Bateman et al., 2015a) or SOA composition difference from different oxidation conditions. As observed in the real atmosphere, aerosol particles are usually a mixture of organic and inorganic species (e.g. sulfate and nitrate; Jimenez et al., 2009). Since the inorganic species have lower glass transition temperature than atmospheric-relevant organics (Pedernera, 2008; Koop et al., 2011), the presence of inorganic species could theoretically lower the glass transition temperature of the estimated SOA compounds mixtures. Furthermore, inorganic species are hydrophilic, and the absorbed water molecules can act as a plasticiser, which effectively lowers the glass transition temperature and softens the aerosol (Koop et al., 2011; Martin, 2000). Therefore, ignoring the mixing with inorganic species, or assuming external mixing as in Shiraiwa et al. (2017), could bias our understanding on the phase behaviour of aerosols containing abundant inorganic compounds.

There are few studies on the phase behaviour of multicomponent aerosol particles. Saukko et al. (2012) found that increasing sulfate fraction mixing with SOA produced by longifolene oxidation can reduce the particle rebounding significantly. Saukko et al. (2015) extended this to study the deliquescence hysteresis of ammonium sulfate with condensed SOA from α-pinene and isoprene oxidation as manifested by

particle rebound. They found the α-pinene SOA condensing on ammonium sulfate seed particles showed no influence on their deliquescence but significantly attenuated the efflorescence behaviour. In contrast, the isoprene SOA system resulted in a loss of sharp deliquescence and efflorescence behaviour in comparison to pure ammonium sulfate (Saukko et al., 2015). These results are partly consistent with similar studies using a different instrument (hygroscopicity tandem differential mobility analyser; Smith et al., 2011; Smith et al., 2012). They found that the α-pinene SOA on ammonium sulfate seed can slightly shift the deliquescence and efflorescence RH by a few percent (Smith et al., 2011), while the isoprene SOA can significantly decrease the deliquescence and efflorescence RH, depending on the organic fraction (Smith et al., 2012). These contrasting findings above indicate that aerosol phase state could differ between different SOA precursor systems and in the presence of inorganic compounds. However, it is still unclear how the phase behaviour (and any associated diffusion limiting behaviour) will be influenced during the formation and evolution of SOA from an increased complexity of mixed precursors in the presence of inorganic seed.

We designed a series of aerosol simulation chamber experiments to study SOA formed from representative biogenic (α-pinene and isoprene) and anthropogenic (o-cresol) VOC photochemistry. The experiments studied single VOC precursors and their binary mixtures under modest NO_x conditions on deliquescent ammonium sulfate seed particles. We frame our results around the following hypotheses:

1. Aerosol phase state for SOA mixture is driven by RH and an organic–inorganic mass ratio.

2. The difference in SOA composition is less important in determining the phase behaviour than the SOA production rate, which changes the organic–inorganic ratio.

The main objective of this paper is to test the above two hypotheses and discuss their potential atmospheric implications.

2 Measurements and methods

2.1 Reaction chamber and experimental set up

The aerosol particles for the experiments were produced in the Manchester Aerosol Chamber (MAC). A detailed description of MAC can be found in Shao et al. (2021), and a brief introduction is given as below. The facility is run as a batch reactor, with an $18\,m^3$ ($3\,m$ (H) $\times$ $3\,m$ (L) $\times$ $2\,m$ (W)) fluorinated ethylene propylene (FEP) Teflon bag supported by three aluminium frames in which the upper and the lower frame can move freely to the expand or collapse as sampling air is introduced to or extracted from the chamber. The Teflon bag is enclosed inside a housing with temperature and relative humidity controlled by an air condition-

ing system. In total, two 6 kW Xenon arc lamps (XBO 6000 W/HSLA OFR; Osram) and a series of halogen bulbs, arranged in seven rows containing 16 bulbs each (Solux 50 W, 4700 K, and Solux MR16, USA), are mounted inside of the enclosure housing. The combination of five rows of halogen bulbs (two rows spare) and two Xenon arc lamps is chosen to be a good representative to mimic the solar spectrum in the wavelength of 290–800 nm (Alfarra et al., 2012). The calculated photolysis rate of NO_2 (j_{NO_2}) from the O_3–NO–NO_2 photostationary state was $(1.8$–$3) \times 10^{-3}\,s^{-1}$ during the experimental period. The simulated irradiation spectrum intensity in our chamber is around a third of the measured solar spectrum at midday on a clear-sky day in Manchester during June (https://www.eurochamp.org/simulation-chambers/MAC-MICC, last access: 24 July 2021).

To ensure chamber cleanliness and data reproducibility, an automatic fill and flush cycle is conducted pre- and post-experiment using $3\,m^3\,s^{-1}$ purified clean air. In total, five to six cycles are routinely conducted between experiments, with the total number concentration of aerosol particles usually lower than 10 particles per cm^{-3} after cleaning. Air is scrubbed using a series of filters, including Purafil (Purafil Inc., USA) and charcoal to remove reactive gaseous compounds and a high-efficiency particulate absorbing (HEPA) filter (Donaldson Company, Inc., USA) to remove particles, and a dryer. To remove reactive compounds, the chamber is soaked in high concentrations of O_3 (~ 1 ppm) overnight between experiments, which is removed during pre-experiment fill and flush cycles on the subsequent day. An additional harsh cleaning procedure is conducted weekly, with high O_3 (~ 1 ppm) and UV for 4–5 h, to consume the remaining reactive compounds.

Seed particles, VOC, NO_x, and water vapour are injected into chamber before illumination. Deliquescent ammonium sulfate (AS) seed (Puratronic; 99.999 % purity) are nebulised and introduced into a drum to mix before flushing into chamber. Liquid VOC precursors (α-pinene, isoprene, and o-cresol; Sigma-Aldrich; gas chromatography (GC) grade with ≥ 99.99 % purity) are injected, using a syringe, into a heated glass bulb in which the VOCs are instantaneously vaporised. The vaporised VOCs are flushed into the chamber with a flow of ~ 0.5 bar high-purity nitrogen (electron capture device (ECD) grade; 99.997 %). Here, the experiments will investigate single and binary mixtures under modest NO_x conditions (VOC/NO_x of 3–10). NO_x (mostly as NO_2 in this study) is introduced through a cylinder with a flow of ~ 0.3 bar high-purity nitrogen (ECD grade; 99.997 %), and the O_3–NO–NO_2 photostationary state will establish immediately after illumination. The detailed initial conditions for the chamber set up are shown in Table 1, and the experimental design will be described in detail in Sect. 2.3.

Table 1. Summary of the initial conditions of chamber experiments.

Experiment date	VOC type	[VOC]$_0$ (ppbv)	VOC/NO$_x$	T (°C)	RH (%)	AS seed conc. (µg m^{-3})*	O : C ratio
28 March 2019	α-pinene	309	7.7	26.7	50.5	72.6	0.36 ± 0.03
17 April 2019	α-pinene	155	4.4	25.9	55.0	47.8	0.45 ± 0.04
2 April 2019	Isoprene	164	6.8	27.2	47.3	64.1	NA
12 April 2019	o-cresol	400	NA	27.3	53.3	47.8	0.64 ± 0.03
19 April 2019	o-cresol	200	5.0	26.9	51.3	51.3	0.66 ± 0.05
8 April 2019	α-pinene/isoprene	237 (155/82)	9.9	27.0	48.4	62.0	0.43 ± 0.05
23 April 2019	α-pinene/o-cresol	355 (155/200)	NA	25.6	55.8	42.5	0.48 ± 0.05
18 April 2019	o-cresol/isoprene	282 (200/82)	8.3	27.1	52.7	49.6	0.69 ± 0.05

* Calculated mass concentration from volume concentration from DMPS, with a density of 1.77 g cm^{-3}. Note: ppbv – parts per billion by volume. NA means no available data due to instrument failure or data lower than the detection limit.

2.2 Instrumentation

A series of instruments are equipped for gas-phase and particle-phase measurements in MAC. NO, NO$_2$, and NO$_x$ are recorded by the NO–NO$_2$–NO$_x$ analyser (model 42i; Thermo Fisher Scientific, USA) and O$_3$ is measured by O$_3$ analyser (model 49C; Thermo Electron Corporation, USA). RH and T inside of MAC are recorded by an EdgeTech dew point hygrometer (DM-C1-DS2-MH-13, USA) and two Sensirion SHT75 sensors (Farnell 413-0698, USA). The aerosol number size distribution (20–550 nm) is measured by a differential mobility particle sizer (DMPS). Hygroscopic growth factor (GF) at 90% RH of submicron aerosol particles (75–250 nm) was recorded by a custom-made hygroscopicity tandem differential mobility analyser (HTDMA; Good et al., 2010), which can be used to calculate the GF at given RH using a κ–Köhler approximation (Petters and Kreidenweis, 2007).

The particle bounce behaviour (bounce fraction; BF) was measured by a three-arm particle rebound apparatus with RH adjustment system. A brief instrumental description is provided below, and more details can be found in Bateman et al. (2014) and Liu et al. (2017), along with a schematic diagram in Fig. S1 in the Supplement of the latter. In total, three single-stage impactors operated in parallel in the system combined with a condensation particle counter (CPC; model 3772; TSI Incorporated, USA). The first impactor is not equipped with a plate (see step 1 in Fig. S1 in Liu et al., 2017), so particles can pass through the first impactor directly, which measures the total particle population (N_1). The second impactor is equipped with a smooth plate (see step 2 in Fig. S1 in Liu et al., 2017), which provides a solid surface and allows particles to rebound from the impactor. The particle population measured after the second impactor represents the sum of particles that do not strike the impactor and that strike but rebound from the impactor (N_2). The third impactor is equipped with a grease-coated plate (see step 3 in Fig. S1 in Liu et al., 2017). The coated grease is quite sticky, and all particles striking the plate will be

stuck. Therefore, the particle number population after grease-coated plate provides a measure of the particles that do not strike the impactor (N_3). The rebound fraction BF is defined in Eq. (1). During the experiments, a differential mobility analyser (DMA) was used to select monodisperse aerosol particles from chamber, with a mobility diameter of 100–200 nm, following the growth of the aerosol particles. The selected particle sizes are larger than the 50 % transmission diameter of the used impactor (84.9 ± 5.4 nm; Bateman et al., 2014) to ensure a reliable bounce fraction measurement.

$$BF = \frac{N_2 - N_3}{N_1 - N_3}. \tag{1}$$

BF can be used as a proxy of aerosol phase state, although it has a limited capability to represent semi-solid or solid particles over 100 Pa s in viscosity (Bateman et al., 2015a; Reid et al., 2018). Nevertheless, it provides insights into the transition process between the liquid and solid or semi-solid phase, referred to as liquid-to-nonliquid transition below.

The chemical composition of the nonrefractory PM$_1$ components (NH$_4^+$, NO$_3^-$, SO$_4^{2-}$, and SOA) was recorded by a high-resolution time-of-flight aerosol mass spectrometer (HR-ToF-AMS; Aerodyne Research, Inc., USA). A detailed introduction of the instrument, calibration procedures, and quantification of the aerosol concentrations was described previously (DeCarlo et al., 2006; Jayne et al., 2000; Allan et al., 2003; Allan et al., 2004). The instrument was operated in "V mode" and recorded with a time resolution of 1 min (30 s mass spectrum (MS) + 30 s particle time of flight – PToF). The elemental ratio of O : C used for the proxy of organic oxidation state and the ions of NO$^+$ and NO$_2^+$ used for the organic nitrate fraction calculation were derived from the high-resolution fitting on V-mode data.

Calibrations were performed before and after the campaign using monodisperse (350 nm) ammonium nitrate and ammonium sulfate particles, following the standard procedure in Jayne et al. (2000) and Jimenez et al. (2003). An averaged ionisation efficiency of ammonium nitrate was 9.38×10^{-8} ions molecule^{-1} from the two calibrations. Ac-

cording to the ion balance of ammonium nitrate and ammonium sulfate in the calibrations, the specific relative ionisation efficiencies (RIE) for NH_4^+ and SO_4^{2-} are determined as 3.57 ± 0.02 and 1.28 ± 0.01, respectively. The RIE of all organic compounds used the default value of 1.4 (Alfarra et al., 2004). In this study, the AMS mass concentrations were corrected by comparing to the real-time DMPS unit mass multiplied by concurrent calculated density from AMS species. The mass ratio of $AMS/(DMPS \times density)$ is 0.4–1.0 in all investigated VOC systems.

2.3 Rationale behind the choice of precursor

The real atmosphere comprises a complex mixture of VOCs with various reactivities, many of which may act as SOA precursors with varying degrees of efficiency. Recent chamber studies have started using relatively simple VOC mixtures to investigate complex interactions in their ability to form SOA in the presence of inorganic seed particles (McFiggans et al., 2019; Shilling et al., 2019). Extending these previous studies, a project was designed that aimed at characterising chemical mechanisms, yield, and physicochemical properties (volatility, hygroscopicity, cloud condensation nuclei (CCN) activity, and phase behaviour) of SOA formed from initially iso-reactive biogenic and/or anthropogenic VOC photochemistry on ammonium sulfate seed and exploring the potential implications for the real atmosphere. Building on McFiggans et al. (2019), we added an anthropogenic VOC (*o*-cresol) into the initially designed binary mixtures of biogenic VOCs (isoprene and α-pinene). *o*-cresol can be emitted into atmosphere both directly, from biomass burning (Coggon et al., 2019; Koss et al., 2018), and indirectly, from the oxidation of toluene (e.g. motor vehicles and solvent use; Fishbein, 1985). Therefore, anthropogenic sources are one of the main contributors to *o*-cresol, but it is worth noting that natural biomass burning can also be an important contributor. *o*-cresol is chosen by virtue of its comparable ·OH reactivity with the chosen biogenic VOCs (Coeur-Tourneur et al., 2006), which enables the comparable initial concentration to have an equal reactivity with ·OH at the beginning of the experiment (referred as iso-reactive). The modest SOA yield of *o*-cresol (Henry et al., 2008) gives a good contrast with the low-yield isoprene and high-yield α-pinene. The overall experiment design enables us to explore the initial SOA formation in iso-reactive single, binary, and ternary VOC mixtures oxidation (details can be found in Voliotis et al., 2021). This paper focuses on the aerosol phase state of seeded SOA from iso-reactive single and binary VOCs photochemistry. Unfortunately, the bounce impactor was unavailable for the ternary mixture experiment.

3 Results and discussion

3.1 BF dependence on RH and organic–inorganic mass ratio

Figure 1 shows the rebound curves of the 100–200 nm multicomponent aerosol particles formed in various VOC systems for the period when the organic mass fraction in NR–PM_1 is larger than 0.05. For all investigated VOC systems, the aerosol particles exhibited BF > 0.8 at RH < 30 % and BF < 0.2 at RH > 80 % at room temperature (18 °C). Between 30 % and 80 % RH, the BF monotonically decreased with the increasing RH, indicating a gradual transition in BF (usually within 15 %–25 % RH width for BF declining from > 0.8 to < 0.2). Assuming the aerosol particles to be nonliquid if their BF > 0.8 and liquid if BF < 0.2 (Bateman et al., 2015a; Liu et al., 2017) implies a gradual transition with RH in all investigated VOC systems, which is in contrast to the rapid dissolution corresponding to the deliquescence of inorganic salt particles (Tang and Munkelwitz, 1993; Kreidenweis and Asa-Awuku, 2014). Owing to limitations of the technique in differentiating particle viscosity at high values (Bateman et al., 2014), the nonliquid phase could represent the semi-solid or solid phase. In addition, the rebound curves varied along with the SOA formation and subsequent evolution as the photochemistry continues in all the investigated VOC systems (as shown in Fig. 1). To illustrate the influences of chemical composition, the overview of the rebound curves as a function of organic–inorganic mass ratio ($MR_{org/inorg}$) in all VOC systems is shown in Fig. S1, indicating the potential important role of $MR_{org/inorg}$ (and maybe the SOA composition) in determining the phase behaviour as RH.

To clearly describe the phase behaviour during SOA formation evolution, the $RH_{BF=0.2}$, $RH_{BF=0.5}$, and $RH_{BF=0.8}$ are determined, representing the RH at which the BF is close to 0.2 (± 0.15), 0.5 (± 0.15), and 0.8 (± 0.15). It is worth noting that the determination of $RH_{BF=0.2, 0.5, 0.8}$ carries a maximum error of ± 5 %, owing to the measurement resolution and resultant number of data points. By tracking the variation in $RH_{BF=0.2, 0.5, 0.8}$ during SOA formation evolution, we can understand the tendency of the phase behaviour change and gain insight into the liquid-to-nonliquid transition for the variation in RH at which BF changes from 0.8 to 0.2 among VOC systems. As different VOCs have different reactivity with the oxidant and yield, the formed SOA mass after 6 h photo-oxidation and, consequently, the $MR_{org/inorg}$ were different among VOC systems. For *o*-cresol/isoprene, 50 % reactivity *o*-cresol, *o*-cresol, α-pinene/isoprene, α-pinene/*o*-cresol, 50 % reactivity α-pinene, and α-pinene systems, and the $MR_{org/inorg}$ reached up to 0.53 ± 0.02, 1.27 ± 0.05, 2.47 ± 0.06, 3.77 ± 0.11, 3.77 ± 0.01, 4.45 ± 0.04, and 7.37 ± 0.06 for the last rebound curve at the end of experiments, respectively. As shown in Fig. 2, the $RH_{BF=0.2, 0.5, 0.8}$ increased towards a maximum as an increase in the $MR_{org/inorg}$ in all investigated VOC systems, indicating an increase in re-
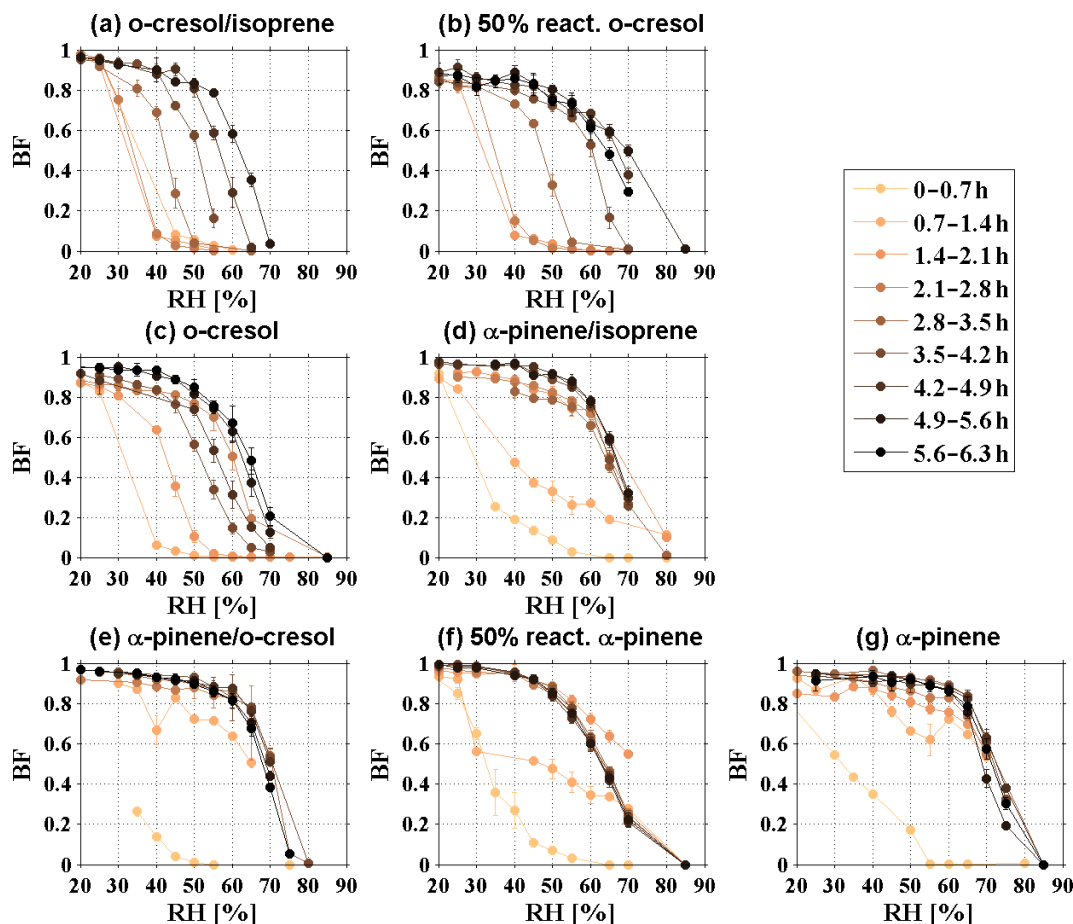
Figure 1. Time series of the bounce fraction (BF) as a function of RH measured by three-arm particle rebound apparatus, with an RH adjustment system of the 100–200 nm secondary organic aerosol (SOA) formed from the photochemistry of various iso-reactive single (binary) biogenic (anthropogenic) VOCs (volatile organic compounds) under modest NO_x conditions on deliquescent ammonium sulfate seed (as the SOA mass fraction in NR–PM$_1$ is larger than 0.05).

bound tendency during the SOA evolution on deliquescent sulfate seed. Figure 2a–c showed a co-increasing trend between RH$_{BF=0.2, 0.5, 0.8}$ and MR$_{org/inorg}$ as MR$_{org/inorg} < 2$; thereafter, RH$_{BF=0.2, 0.5, 0.8}$ remained constant at 70 %–75 %, 65 %–70 %, and 50 %–65 %, respectively, in all VOC systems. Herein, the reason for the decrease in RH$_{BF=0.5}$ from 60 % to 50 % at MR$_{org/inorg} \sim 1$ in the o-cresol system was not known, and the same behaviour was not observed for RH$_{BF=0.2, 0.8}$.

As expected, the change in MR$_{org/inorg}$ during SOA formation and evolution differed in various VOC systems (as shown in Fig. 3), depending on their SOA production rate (as shown in Fig. S2) and noting the comparable initial sulfate seed concentrations. The order of the SOA production rate (from low to high) in all the investigated VOC systems was o-cresol/isoprene < 50 % reactivity o-cresol < o-cresol < α-pinene/isoprene < α-pinene/o-cresol < 50 % reactivity α-pinene < α-pinene (note that insufficient mass was generated from the isoprene system). It is worth noting that

the SOA production rate in α-pinene/isoprene, α-pinene/o-cresol, and 50 % reactivity α-pinene systems are very similar, and their order is determined by the minor difference in the slopes in Fig. S2. Clearly, a higher SOA production rate increased the MR$_{org/inorg}$ faster, causing the phase behaviour change. As shown in Fig. 4, RH$_{BF=0.2, 0.5, 0.8}$ showed an increasing trend towards a maximum across the various VOC systems, which is highly related to how fast the SOA were formed. With an increasing SOA formation rate from the lowest o-cresol/isoprene to the highest α-pinene system, a shorter time was taken for RH$_{BF=0.2, 0.5, 0.8}$ to reach the maximum. Take RH$_{BF=0.5}$ as an example; it can be seen from Fig. 1 that the RH$_{BF=0.5}$ at the beginning of the photochemistry was lower than 40 % for all investigated VOC systems. Figure 4b shows that, for the o-cresol/isoprene system with the lowest SOA formation rate, it took ~ 3.5 h for RH$_{BF=0.5}$ to increase to 50 % and ~ 5 h to approach 60 %. For comparison, for α-pinene/isoprene (the moderate) and α-pinene (the highest) systems, it takes only ~ 1.5 and 0.5 h for the
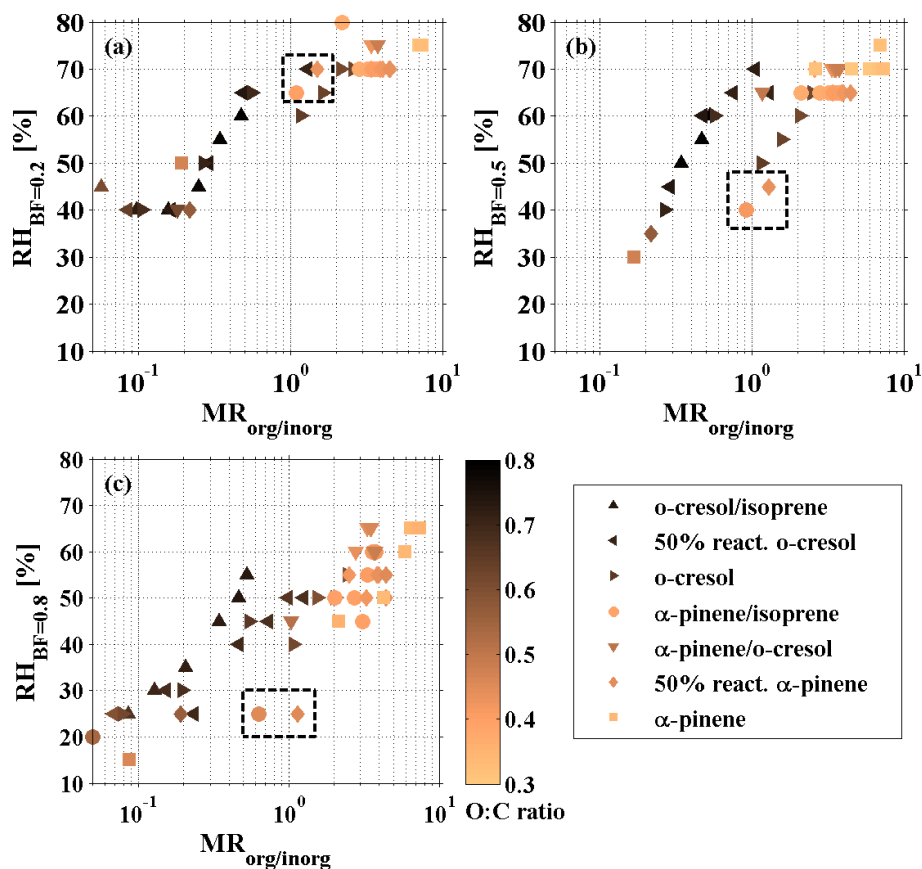
Figure 2. The measured **(a)** $RH_{BF=0.2}$, **(b)** $RH_{BF=0.5}$, and **(c)** $RH_{BF=0.8}$ as a function of the organic–inorganic ratio ($MR_{org/inorg}$), coloured by the atomic O : C ratio in the photochemistry of various VOC systems on deliquescent ammonium sulfate seed. The black box points out the $RH_{BF=0.2,\,0.5,\,0.8}$ at moderate $MR_{org/inorg}$ of ~ 1 for biogenic VOC systems (α-pinene/isoprene; 50 % reactivity α-pinene).

$RH_{BF=0.5}$ to increase to 50 % and 70 %, respectively. Similar results can also be found for the cases in $RH_{BF=0.2,\,0.8}$.

It can be seen that, in all of the investigated VOC systems, when the SOA mass fraction was > 0.05, the phase dependence on $MR_{org/inorg}$ was qualitatively similar, irrespective of the single (binary) biogenic (anthropogenic) SOA precursors. That is, the $RH_{BF=0.2,\,0.5,\,0.8}$ increased towards a maximum value with an increase in the $MR_{org/inorg}$ during the SOA formation evolution. With regard to the SOA from biogenic or anthropogenic VOCs, oxidation showed an amorphous solid property rather than the expected liquid phase as deliquescent inorganic particles (Bateman et al., 2015a; Virtanen et al., 2010; Saukko et al., 2015; Saukko et al., 2012), such as the $RH_{BF=0.2,\,0.5,\,0.8}$ of SOA formed from α-pinene and toluene photo-oxidation, were 80 %–90 %, 80 %–85 %, and ~ 65 %, respectively (Bateman et al., 2015a). It is expected that the increasing aerosol rebounding tendency can happen with increasing SOA mass condensing on the deliquescent sulfate seed. This speculation is supported by our results which show an increase in $RH_{BF=0.2,\,0.5,\,0.8}$ toward the maximum with more SOA condensation. Additionally, the maximum $RH_{BF=0.2,\,0.5,\,0.8}$ at high $MR_{org/inorg}$ of ~ 8 in

our study was 10 %–15 % lower than SOA mentioned above, indicating that the presence of a small mass fraction of inorganic compounds (~ 10 %) makes multicomponent aerosol particles bounce less than the SOA. Moreover, the time taken for $RH_{BF=0.2,\,0.5,\,0.8}$ to reach the maximum depended on how rapidly the SOA was formed, i.e. there was a shorter time for the faster SOA production rate of the investigated VOC systems. This general behaviour was independent of the yield of the VOC and whether the precursor was biogenic or anthropogenic. In addition, the individual VOC systems behaved in the same way as the VOC mixtures.

As shown in Fig. 3, it should be noted that, to avoid a high signal-to-noise ratio (SNR) for low organic mass loading measured by HR-ToF-AMS, the data points with an organic mass fraction larger than 0.05 (assuming uniform chemical composition) were selected for consideration. It was observed that particulate nitrate (maximum 5 %–16 % of NR–PM_1) was formed during photochemistry in all investigated VOC systems. Nitrate can either be formed from the oxidation of NO_2, followed by the neutralisation of NH_3, or an organic oxidation product (organic nitrate). The organic nitrate fraction in the total nitrate signal can be estimated
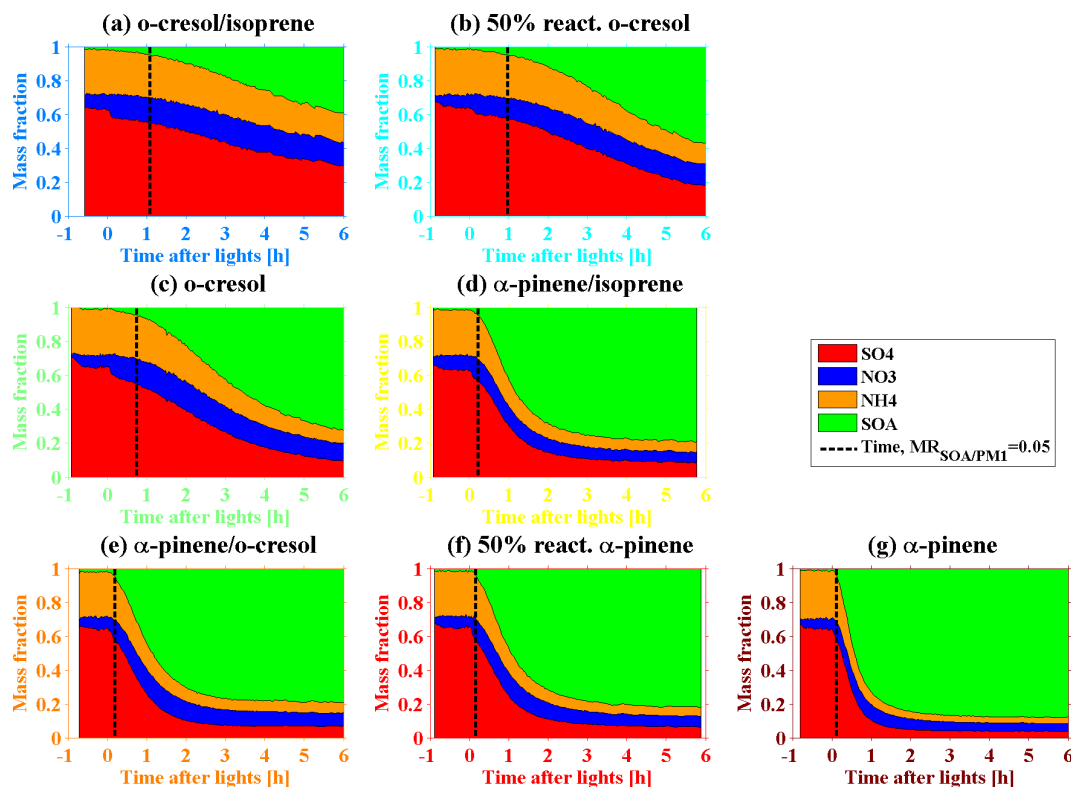
Figure 3. Summary of mass fraction of chemical species (SO$_4$, NO$_3$, NH$_4$, and SOA) in bulk NR–PM$_1$ measured by HR-ToF-AMS in the photochemistry of various VOC systems on deliquescent ammonium sulfate seed. The black dashed line represents the defined time at which the SOA mass fraction is 0.05.

following the NO$^+$/NO$_2^+$ ratio method proposed by Farmer et al. (2010), given the differentiation of the NO$^+$/NO$_2^+$ ratio for pure NH$_4$NO$_3$ (2.6; from calibrations) and organic nitrate of 10–15 (Bruns et al., 2010; Fry et al., 2009; Kiendler-Scharr et al., 2016; Reyes-Villegas et al., 2018). As shown in Fig. S3, the organic nitrate fraction in the total nitrate signal was lower than 20 % in almost all investigated VOC systems, except for the last 2 h of *o*-cresol system (up to ∼ 26 %). This NO$^+$/NO$_2^+$ ratio method can indicate organic nitrate statistically only if the organic nitrate fraction is larger than 15 % (Bruns et al., 2010). Thus, the observed particulate nitrate is mainly inorganic nitrate with a small contribution of organic nitrate (< 20 %) for all VOC systems in this study. The small contribution of organic nitrate mass has little influence on the onset of the organic mass fraction > 0.05. Moreover, Li et al. (2017) found that the pure NH$_4$NO$_3$ particles adhered on the impactor even though the RH had been reduced to ∼ 5 %. It is worth noting that the variable particulate nitrate across all VOC systems in this study might have some influence on the phase behaviour of the multicomponent aerosol particles during SOA formation evolution, and the influence of changing inorganic component ratios on the BF in multicomponent mixtures should be the focus of this work.

## 3.2	BF dependence on OA composition

In addition to the control of the BF by MR$_{org/inorg}$, there is an indication that the SOA composition across the various VOC systems may also impact the aerosol phase state. As indicated in Fig. 2b and c, the increase in the RH$_{BF=0.5, 0.8}$ as a function of MR$_{org/inorg}$ is less rapid in the *α*-pinene/isoprene, 50 % reactivity *α*-pinene, and the *α*-pinene system (referred to as biogenic volatile organic compound (BVOC) systems, which are anthropogenic free) than the anthropogenic VOC (AVOC) systems (AVOC-containing systems, including *o*-cresol, 50 % reactivity *o*-cresol, *o*-cresol/isoprene, and *α*-pinene/*o*-cresol). It can be seen that, for the AVOC-containing systems, the RH$_{BF=0.5}$ and RH$_{BF=0.8}$ were 65 %–70 % and 40 %–55 % when MR$_{org/inorg}$ approached ∼ 1, whereas there was only 40 %–45 % and ∼ 25 % in the 50 % reactivity *α*-pinene and *α*-pinene/isoprene systems (BVOC systems). Interestingly, with more SOA condensing, the discrepancy disappeared, and the RH$_{BF=0.5}$ and RH$_{BF=0.8}$ converged for BVOC and AVOC-containing systems as the MR$_{org/inorg}$ > 2. In contrast, the RH$_{BF=0.2}$ as a function of MR$_{org/inorg}$ was the same for BVOC and AVOC-containing mixtures. This indicates that the decrease in RH to achieve the liquid-to-nonliquid transition for BVOC and AVOC-
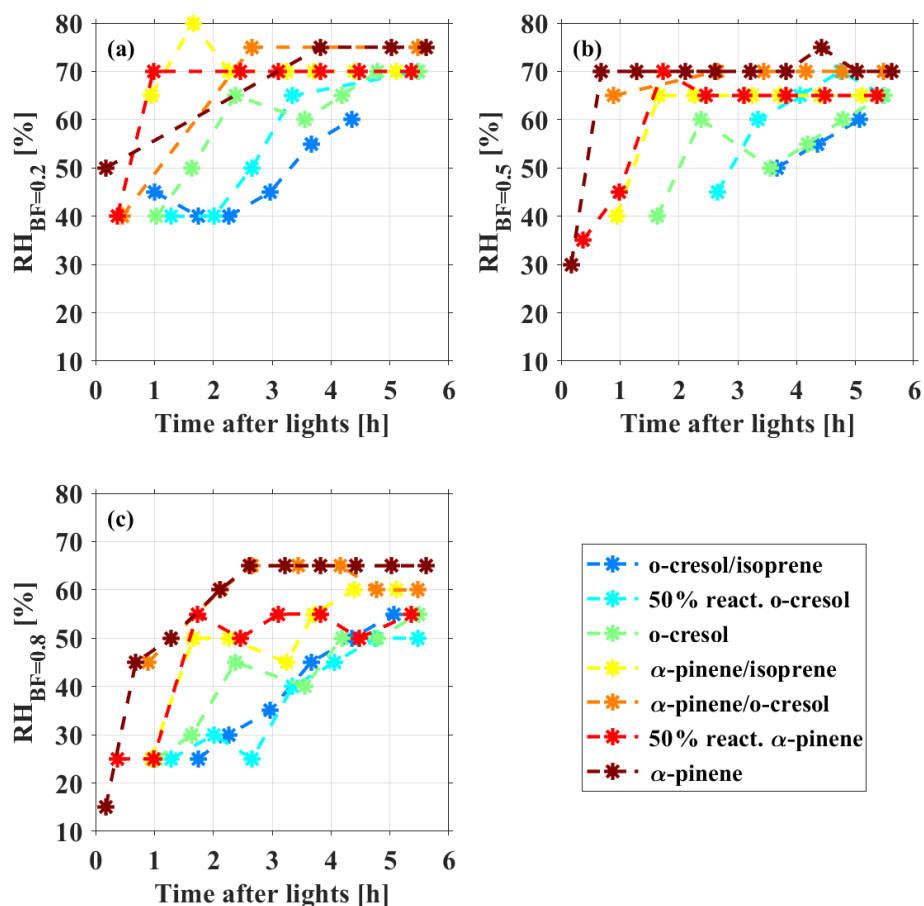
Figure 4. The time series of measured **(a)** $RH_{BF=0.2}$, **(b)** $RH_{BF=0.5}$, and **(c)** $RH_{BF=0.8}$ of the multicomponent aerosol particles in the photochemistry of various VOC systems on deliquescent ammonium sulfate seed.

containing systems was different at moderate $MR_{org/inorg}$ of ~ 1 but quantitatively similar at low and high $MR_{org/inorg}$.

The above evidence indicates that the VOC type (BVOC or AVOC-containing systems), and then SOA composition, can play a second-order role in the phase behaviour of multicomponent aerosol particles. Here, we used degree of oxidation of the SOA (O : C atomic ratio derived from HR-ToF-AMS) as a proxy of SOA composition to explore its relationship with phase behaviour. As shown in Table 1, for BVOC systems the averaged atomic O : C ratio of SOA in α-pinene/isoprene, 50 % reactivity α-pinene, and α-pinene systems was 0.43 ± 0.05, 0.45 ± 0.04, and 0.36 ± 0.03, respectively. For AVOC-containing systems, the O : C ratio of SOA was 10 %–50 % higher than BVOC systems, with 0.69 ± 0.05, 0.66 ± 0.05, 0.64 ± 0.03, 0.48 ± 0.05 in o-cresol/isoprene, 50 % reactivity o-cresol, o-cresol and α-pinene/o-cresol systems, respectively. In addition, the $RH_{BF=0.2,\,0.5,\,0.8}$ response to the $MR_{org/inorg}$ was coloured according to the O : C ratio in Fig. 2. The O : C ratio was characteristic for the SOA precursors and showed little variation through individual experiments. No direct relationship between O : C ratio and the phase behaviour change was observed during the SOA for-

mation evolution among all investigated VOC systems. Previous studies have shown a tentative dependence on the O : C ratio of the organic particles with phase behaviour (e.g. glass transition temperature; Koop et al., 2011; Shiraiwa et al., 2017). In contrast, Saukko et al. (2012) showed that the O : C ratio only influenced rebounding behaviour of SOA formed from n-heptadecane in a potential aerosol mass (PAM) reactor, with no influence in the α-pinene, longifolene, and naphthalene systems. There was some evidence showing that aerosol morphology (single well-mixed phase or phase separation) was closely related to the O : C ratio of SOA and the organic–inorganic mass ratio (Bertram et al., 2011; Krieger et al., 2012; You et al., 2014; Freedman, 2017; Song et al., 2012; Smith et al., 2013). It is unknown whether the morphology plays a role in the phase behaviour discrepancy between BVOC and AVOC-containing systems at moderate $MR_{org/inorg}$, considering their O : C difference; nevertheless, this is of interest and needs further investigation.
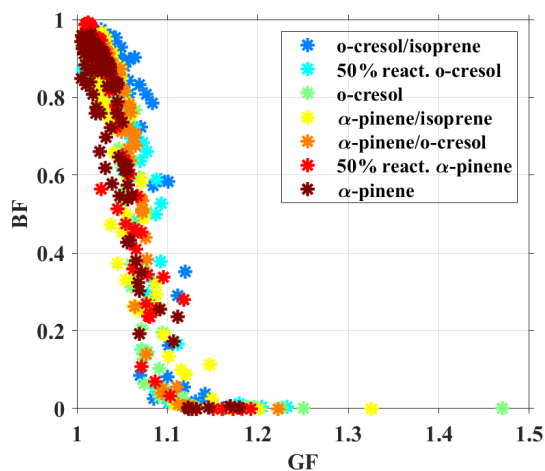
Figure 5. The relation of BF and hygroscopic GF of aerosol particles during 6 h photochemistry experiments in various VOC systems.

3.3 Mixing role of chemical composition and RH on BF

As we know that the chemical composition and RH are key factors influencing aerosol water uptake at a given size (Kreidenweis and Asa-Awuku, 2014). To discuss the mixing role of the chemical composition and RH on BF, the GF at the RH of the BF measurement was calculated from the HTDMA measurement using the κ–Köhler equation, and the relation between the BF and the GF was plotted in Fig. 5. It can be seen that the BF showed a monotonic decrease from ~ 1 to ~ 0 with the increasing GF from ~ 1 to ~ 1.15 in all VOC systems. As the GF is larger than 1.15, the aerosol particles are kept in the liquid phase (BF ~ 0). This evidence indicated the key role of increasing the aerosol water uptake in the phase transition from nonliquid to liquid. The BF–GF relation of the varying multicomponent aerosol particles, including SOA and inorganic compounds, is comparable with a previous study (Bateman et al., 2015a). They measured the BF of the SOA from α-pinene, toluene, and isoprene and found that the BF is nearly 0 when the GF is larger than > 1.15 (Bateman et al., 2015a).

4 Conclusions and implications

Our experiments support the validity of our two proposed hypotheses, namely that (1) the aerosol phase state for SOA mixture is determined by RH and the organic–inorganic mass ratio (MR$_{org/inorg}$). (2) The difference in the SOA composition is less important for determining the phase behaviour than the rate of SOA production, which changes the MR$_{org/inorg}$.

First, aerosol phase state is clearly RH dependent, as is already widely known. Multicomponent aerosol particles were always found to exhibit liquid-like behaviour (BF < 0.2)

above 80 % RH and nonliquid-like behaviour (BF > 0.8) below 30 % RH. The bounce measurements always indicated continuously increasing nonliquid-like behaviour as RH decreased from 80 % to 30 %. These RH-dependent rebound curves strongly depended on the increase in MR$_{org/inorg}$ during SOA formation in all investigated VOC systems. The identified RH$_{BF=0.2, 0.5, 0.8}$ increased towards a maximum with the increase in the MR$_{org/inorg}$, and the increase in the rate of RH$_{BF=0.2, 0.5, 0.8}$ is determined by the SOA production rate on sulfate seed across the VOC systems. This general behaviour was independent of the yield of the SOA precursors and whether the precursor was biogenic or anthropogenic. In some ways, this is an obvious result that follows from the rate of the SOA mass increase in the system under investigation. However, this production rate will be dependent on the reactivity and yield of VOCs in the mixture and their concentrations and interactions influencing SOA mass formation. This set of complex dependencies will control the changes in particle MR$_{org/inorg}$ in mixtures and, hence, in phase behaviour.

Although less important than the RH and MR$_{org/inorg}$, the SOA composition plays a secondary role affecting the phase behaviour. It was observed that the RH$_{BF=0.2}$ as a function of MR$_{org/inorg}$ was the same for BVOC (AVOC free) and AVOC-containing systems; however, the decrease in RH to achieve a liquid-to-nonliquid transition (BF from ~ 0.2 to ~ 0.8) was different at moderate MR$_{org/inorg}$ of ~ 1 but quantitatively similar at low and high MR$_{org/inorg}$. For example, at a moderate MR$_{org/inorg}$ of ~ 1, the RH$_{BF=0.2}$ for BVOC and AVOC-containing systems was 65 %–70 %. To achieve a liquid-to-nonliquid transition with a BF of ~ 0.8, the RH needed to decrease to 40 %–55 % in AVOC-containing systems but to ~ 25 % in BVOC systems. This discrepancy cannot be explained by the atomic O : C ratio of SOA during SOA formation evolution. It should be the focus of future work to investigate whether SOA composition has a more pronounced effect outside the dynamic O : C range of the mixtures in our experiments. Additionally, by combining the chemical composition and RH, we calculated the hygroscopic growth factor (GF) and found its key role in impacting phase behaviour. The multicomponent aerosol particles were liquid in all VOC systems when the GF was higher than 1.15 at room temperature and transmitted from liquid to nonliquid when the GF decreased to ~ 1.

Multicomponent aerosol phase state depends on RH and the organic–inorganic mass ratio in a particle and in the atmosphere, as well as in our chamber. Any interactions influencing these two factors will, therefore, influence the phase behaviour. For example, a fast formation of SOA or a significant ambient RH change in the real atmosphere could change phase behaviour of particles and, consequently, influence atmospheric physicochemical processes. There is an additional indication that an increased anthropogenic VOC contribution to the mixture could give different phase behaviour at a certain moderate organic mass fraction (~ 50 %); hence, there will be some second-order differences depending on the rel-

ative contributions of anthropogenic and biogenic VOC. Further studies should be carried out on more complex and realistic atmospheric mixtures.

References

Alfarra, M. R., Coe, H., Allan, J. D., Bower, K. N., Boudries, H., Canagaratna, M. R., Jimenez, J. L., Jayne, J. T., Garforth, A. A., Li, S.-M., and Worsnop, D. R.: Characterization of urban and rural organic particulate in the Lower Fraser Valley using two Aerodyne Aerosol Mass Spectrometers, Atmos. Environ., 38, 5745–5758, https://doi.org/10.1016/j.atmosenv.2004.01.054, 2004.

Alfarra, M. R., Hamilton, J. F., Wyche, K. P., Good, N., Ward, M. W., Carr, T., Barley, M. H., Monks, P. S., Jenkin, M. E., Lewis, A. C., and McFiggans, G. B.: The effect of photochemical ageing and initial precursor concentration on the composition and hygroscopic properties of β-caryophyllene secondary organic aerosol, Atmos. Chem. Phys., 12, 6417–6436, https://doi.org/10.5194/acp-12-6417-2012, 2012.

Allan, J. D., Jimenez, J. L., Williams, P. I., Alfarra, M. R., Bower, K. N., Jayne, J. T., Coe, H., and Worsnop, D. R.: Quantitative sampling using an Aerodyne aerosol mass spectrometer 1. Techniques of data interpretation and error analysis, J. Geophys. Res.-Atmos., 108, 4090, https://doi.org/10.1029/2002jd002358, 2003.

Allan, J. D., Delia, A. E., Coe, H., Bower, K. N., Alfarra, M. R., Jimenez, J. L., Middlebrook, A. M., Drewnick, F., Onasch, T. B., Canagaratna, M. R., Jayne, J. T., and Worsnop, D. R.: A generalised method for the extraction of chemically resolved mass spectra from Aerodyne aerosol mass spectrometer data, J. Aerosol Sci., 35, 909–922, https://doi.org/10.1016/j.jaerosci.2004.02.007, 2004.

Bateman, A. P., Belassein, H., and Martin, S. T.: Impactor Apparatus for the Study of Particle Rebound: Relative Humidity and Capillary Forces, Aerosol Sci. Tech., 48, 42–52, https://doi.org/10.1080/02786826.2013.853866, 2014.

Bateman, A. P., Bertram, A. K., and Martin, S. T.: Hygroscopic Influence on the Semisolid-to-Liquid Transition of Secondary Organic Materials, J. Phys. Chem. A, 119, 4386–4395, https://doi.org/10.1021/jp508521c, 2015a.

Bateman, A. P., Gong, Z., Liu, P., Sato, B., Cirino, G., Zhang, Y., Artaxo, P., Bertram, A. K., Manzi, A. O., Rizzo, L. V., Souza, R. A. F., Zaveri, R. A., and Martin, S. T.: Sub-micrometre particulate matter is primarily in liquid form over Amazon rainforest, Nat. Geosci., 9, 34, https://doi.org/10.1038/ngeo2599, 2015b.

Bateman, A. P., Gong, Z., Harder, T. H., de Sá, S. S., Wang, B., Castillo, P., China, S., Liu, Y., O'Brien, R. E., Palm, B. B., Shiu, H.-W., Cirino, G. G., Thalman, R., Adachi, K., Alexander, M. L., Artaxo, P., Bertram, A. K., Buseck, P. R., Gilles, M. K., Jimenez, J. L., Laskin, A., Manzi, A. O., Sedlacek, A., Souza, R. A. F., Wang, J., Zaveri, R., and Martin, S. T.: Anthropogenic influences on the physical state of submicron particulate matter over a tropical forest, Atmos. Chem. Phys., 17, 1759–1773, https://doi.org/10.5194/acp-17-1759-2017, 2017.

Bertram, A. K., Martin, S. T., Hanna, S. J., Smith, M. L., Bodsworth, A., Chen, Q., Kuwata, M., Liu, A., You, Y., and Zorn, S. R.: Predicting the relative humidities of liquid-liquid

phase separation, efflorescence, and deliquescence of mixed particles of ammonium sulfate, organic material, and water using the organic-to-sulfate mass ratio of the particle and the oxygen-to-carbon elemental ratio of the organic component, Atmos. Chem. Phys., 11, 10995–11006, https://doi.org/10.5194/acp-11-10995-2011, 2011.

Bruns, E. A., Perraud, V., Zelenyuk, A., Ezell, M. J., Johnson, S. N., Yu, Y., Imre, D., Finlayson-Pitts, B. J., and Alexander, M. L.: Comparison of FTIR and Particle Mass Spectrometry for the Measurement of Particulate Organic Nitrates, Environ. Sci. Technol., 44, 1056–1061, https://doi.org/10.1021/es9029864, 2010.

Coeur-Tourneur, C., Henry, F., Janquin, M.-A., and Brutier, L.: Gas-phase reaction of hydroxyl radicals with m-, o- and p-cresol, Int. J. Chem. Kinet., 38, 553–562, https://doi.org/10.1002/kin.20186, 2006.

Coggon, M. M., Lim, C. Y., Koss, A. R., Sekimoto, K., Yuan, B., Gilman, J. B., Hagan, D. H., Selimovic, V., Zarzana, K. J., Brown, S. S., Roberts, J. M., Müller, M., Yokelson, R., Wisthaler, A., Krechmer, J. E., Jimenez, J. L., Cappa, C., Kroll, J. H., de Gouw, J., and Warneke, C.: OH chemistry of non-methane organic gases (NMOGs) emitted from laboratory and ambient biomass burning smoke: evaluating the influence of furans and oxygenated aromatics on ozone and secondary NMOG formation, Atmos. Chem. Phys., 19, 14875–14899, https://doi.org/10.5194/acp-19-14875-2019, 2019.

Dahneke, B.: The capture of aerosol particles by surfaces, J. Colloid Interf. Sci., 37, 342–353, https://doi.org/10.1016/0021-9797(71)90302-X, 1971.

DeCarlo, P. F., Kimmel, J. R., Trimborn, A., Northway, M. J., Jayne, J. T., Aiken, A. C., Gonin, M., Fuhrer, K., Horvath, T., Docherty, K. S., Worsnop, D. R., and Jimenez, J. L.: Field-Deployable, High-Resolution, Time-of-Flight Aerosol Mass Spectrometer, Anal. Chem., 78, 8281–8289, https://doi.org/10.1021/ac061249n, 2006.

Farmer, D. K., Matsunaga, A., Docherty, K. S., Surratt, J. D., Seinfeld, J. H., Ziemann, P. J., and Jimenez, J. L.: Response of an aerosol mass spectrometer to organonitrates and organosulfates and implications for atmospheric chemistry, P. Natl. Acad. Sci. USA, 107, 6670–6675, https://doi.org/10.1073/pnas.0912340107, 2010.

Fishbein, L.: An overview of environmental and toxicological aspects of aromatic hydrocarbons II. Toluene, Sci. Total Environ., 42, 267–288, https://doi.org/10.1016/0048-9697(85)90062-2, 1985.

Freedman, M. A.: Phase separation in organic aerosol, Chem. Soc. Rev., 46, 7694–7705, https://doi.org/10.1039/C6CS00783J, 2017.

Fry, J. L., Kiendler-Scharr, A., Rollins, A. W., Wooldridge, P. J., Brown, S. S., Fuchs, H., Dubé, W., Mensah, A., dal Maso, M., Tillmann, R., Dorn, H.-P., Brauers, T., and Cohen, R. C.: Organic nitrate and secondary organic aerosol yield from NO_3 oxidation of β-pinene evaluated using a gas-phase kinetics/aerosol partitioning model, Atmos. Chem. Phys., 9, 1431–1449, https://doi.org/10.5194/acp-9-1431-2009, 2009.

Good, N., Coe, H., and McFiggans, G.: Instrumentational operation and analytical methodology for the reconciliation of aerosol water uptake under sub- and supersaturated conditions, Atmos. Meas. Tech., 3, 1241–1254, https://doi.org/10.5194/amt-3-1241-2010, 2010.

Henry, F., Coeur-Tourneur, C., Ledoux, F., Tomas, A., and Menu, D.: Secondary organic aerosol formation from the gas phase reaction of hydroxyl radicals with m-, o- and p-cresol, Atmos. Environ., 42, 3035–3045, https://doi.org/10.1016/j.atmosenv.2007.12.043, 2008.

Ignatius, K., Kristensen, T. B., Järvinen, E., Nichman, L., Fuchs, C., Gordon, H., Herenz, P., Hoyle, C. R., Duplissy, J., Garimella, S., Dias, A., Frege, C., Höppel, N., Tröstl, J., Wagner, R., Yan, C., Amorim, A., Baltensperger, U., Curtius, J., Donahue, N. M., Gallagher, M. W., Kirkby, J., Kulmala, M., Möhler, O., Saathoff, H., Schnaiter, M., Tomé, A., Virtanen, A., Worsnop, D., and Stratmann, F.: Heterogeneous ice nucleation of viscous secondary organic aerosol produced from ozonolysis of α-pinene, Atmos. Chem. Phys., 16, 6495–6509, https://doi.org/10.5194/acp-16-6495-2016, 2016.

Jayne, J. T., Leard, D. C., Zhang, X., Davidovits, P., Smith, K. A., Kolb, C. E., and Worsnop, D. R.: Development of an Aerosol Mass Spectrometer for Size and Composition Analysis of Submicron Particles, Aerosol Sci. Tech., 33, 49–70, https://doi.org/10.1080/027868200410840, 2000.

Jimenez, J. L., Jayne, J. T., Shi, Q., Kolb, C. E., Worsnop, D. R., Yourshaw, I., Seinfeld, J. H., Flagan, R. C., Zhang, X., Smith, K. A., Morris, J. W., and Davidovits, P.: Ambient aerosol sampling using the Aerodyne Aerosol Mass Spectrometer, J. Geophys. Res.-Atmos., 108, https://doi.org/10.1029/2001JD001213, 2003.

Jimenez, J. L., Canagaratna, M. R., Donahue, N. M., Prevot, A. S. H., Zhang, Q., Kroll, J. H., DeCarlo, P. F., Allan, J. D., Coe, H., Ng, N. L., Aiken, A. C., Docherty, K. S., Ulbrich, I. M., Grieshop, A. P., Robinson, A. L., Duplissy, J., Smith, J. D., Wilson, K. R., Lanz, V. A., Hueglin, C., Sun, Y. L., Tian, J., Laaksonen, A., Raatikainen, T., Rautiainen, J., Vaattovaara, P., Ehn, M., Kulmala, M., Tomlinson, J. M., Collins, D. R., Cubison, M. J., Dunlea, J., Huffman, J. A., Onasch, T. B., Alfarra, M. R., Williams, P. I., Bower, K., Kondo, Y., Schneider, J., Drewnick, F., Borrmann, S., Weimer, S., Demerjian, K., Salcedo, D., Cottrell, L., Griffin, R., Takami, A., Miyoshi, T., Hatakeyama, S., Shimono, A., Sun, J. Y., Zhang, Y. M., Dzepina, K., Kimmel, J. R., Sueper, D., Jayne, J. T., Herndon, S. C., Trimborn, A. M., Williams, L. R., Wood, E. C., Middlebrook, A. M., Kolb, C. E., Baltensperger, U., and Worsnop, D. R.: Evolution of Organic Aerosols in the Atmosphere, Science, 326, 1525–1529, https://doi.org/10.1126/science.1180353, 2009.

Kiendler-Scharr, A., Mensah, A. A., Friese, E., Topping, D., Nemitz, E., Prevot, A. S. H., Äijälä, M., Allan, J., Canonaco, F., Canagaratna, M., Carbone, S., Crippa, M., Dall Osto, M., Day, D. A., De Carlo, P., Di Marco, C. F., Elbern, H., Eriksson, A., Freney, E., Hao, L., Herrmann, H., Hildebrandt, L., Hillamo, R., Jimenez, J. L., Laaksonen, A., McFiggans, G., Mohr, C., O'Dowd, C., Otjes, R., Ovadnevaite, J., Pandis, S. N., Poulain, L., Schlag, P., Sellegri, K., Swietlicki, E., Tiitta, P., Vermeulen, A., Wahner, A., Worsnop, D., and Wu, H.-C.: Ubiquity of organic nitrates from nighttime chemistry in the European submicron aerosol, Geophys. Res. Lett., 43, 7735–7744, https://doi.org/10.1002/2016gl069239, 2016.

Koop, T., Bookhold, J., Shiraiwa, M., and Poschl, U.: Glass transition and phase state of organic compounds: dependency on molecular properties and implications for secondary organic

aerosols in the atmosphere, Phys. Chem. Chem. Phys., 13, 19238–19255, https://doi.org/10.1039/C1CP22617G, 2011.

Koss, A. R., Sekimoto, K., Gilman, J. B., Selimovic, V., Coggon, M. M., Zarzana, K. J., Yuan, B., Lerner, B. M., Brown, S. S., Jimenez, J. L., Krechmer, J., Roberts, J. M., Warneke, C., Yokelson, R. J., and de Gouw, J.: Non-methane organic gas emissions from biomass burning: identification, quantification, and emission factors from PTR-ToF during the FIREX 2016 laboratory experiment, Atmos. Chem. Phys., 18, 3299–3319, https://doi.org/10.5194/acp-18-3299-2018, 2018.

Kreidenweis, S. and Asa-Awuku, A.: Aerosol Hygroscopicity: Particle Water Content and Its Role in Atmospheric Processes, Elsevier Science, Sciencedirect, 331–361, 2014.

Krieger, U. K., Marcolli, C., and Reid, J. P.: Exploring the complexity of aerosol particle properties and processes using single particle techniques, Chem. Soc. Rev., 41, 6631–6662, https://doi.org/10.1039/C2CS35082C, 2012.

Kuwata, M. and Martin, S. T.: Phase of atmospheric secondary organic material affects its reactivity, P. Natl. Acad. Sci. USA, 109, 17354–17359, https://doi.org/10.1073/pnas.1209071109, 2012.

Li, Y. J., Liu, P. F., Bergoend, C., Bateman, A. P., and Martin, S. T.: Rebounding hygroscopic inorganic aerosol particles: Liquids, gels, and hydrates, Aerosol Sci. Tech., 51, 388–396, https://doi.org/10.1080/02786826.2016.1263384, 2017.

Liu, Y., Wu, Z., Wang, Y., Xiao, Y., Gu, F., Zheng, J., Tan, T., Shang, D., Wu, Y., Zeng, L., Hu, M., Bateman, A. P., and Martin, S. T.: Submicrometer Particles Are in the Liquid State during Heavy Haze Episodes in the Urban Atmosphere of Beijing, China, Environ. Sci. Tech. Lett., 4, 427–432, https://doi.org/10.1021/acs.estlett.7b00352, 2017.

Liu, Y., Wu, Z., Huang, X., Shen, H., Bai, Y., Qiao, K., Meng, X., Hu, W., Tang, M., and He, L.: Aerosol Phase State and Its Link to Chemical Composition and Liquid Water Content in a Subtropical Coastal Megacity, Environ. Sci. Technol., 53, 5027–5033, https://doi.org/10.1021/acs.est.9b01196, 2019.

MAC/NCAS-MAN – Manchester chamber group: SOA from mixed precursors, available at: https://data.eurochamp.org/data-access/chamber-experiments/, last access date: 24 July 2021.

Martin, S. T.: Phase Transitions of Aqueous Atmospheric Particles, Chem. Rev., 100, 3403–3454, https://doi.org/10.1021/cr990034t, 2000.

McFiggans, G., Mentel, T. F., Wildt, J., Pullinen, I., Kang, S., Kleist, E., Schmitt, S., Springer, M., Tillmann, R., Wu, C., Zhao, D., Hallquist, M., Faxon, C., Le Breton, M., Hallquist, Å. M., Simpson, D., Bergström, R., Jenkin, M. E., Ehn, M., Thornton, J. A., Alfarra, M. R., Bannan, T. J., Percival, C. J., Priestley, M., Topping, D., and Kiendler-Scharr, A.: Secondary organic aerosol reduced by mixture of atmospheric vapours, Nature, 565, 587–593, https://doi.org/10.1038/s41586-018-0871-y, 2019.

Murray, B. J.: Inhibition of ice crystallisation in highly viscous aqueous organic acid droplets, Atmos. Chem. Phys., 8, 5423–5433, https://doi.org/10.5194/acp-8-5423-2008, 2008.

Murray, B. J., Wilson, T. W., Dobbie, S., Cui, Z., Al-Jumur, S. M. R. K., Möhler, O., Schnaiter, M., Wagner, R., Benz, S., Niemand, M., Saathoff, H., Ebert, V., Wagner, S., and Kärcher, B.: Heterogeneous nucleation of ice particles on glassy aerosols under cirrus conditions, Nat. Geosci., 3, 233, https://doi.org/10.1038/ngeo817, 2010.

Pajunoja, A., Hu, W., Leong, Y. J., Taylor, N. F., Miettinen, P., Palm, B. B., Mikkonen, S., Collins, D. R., Jimenez, J. L., and Virtanen, A.: Phase state of ambient aerosol linked with water uptake and chemical aging in the southeastern US, Atmos. Chem. Phys., 16, 11163–11176, https://doi.org/10.5194/acp-16-11163-2016, 2016.

Pedernera, D. A.: Glass formation in upper tropospheric aerosol particles, PhD thesis, Bielefeld University, available at: http://pub.uni-bielefeld.de/publication/2303351 (last access: 24 July 2021), 2008.

Petters, M. D. and Kreidenweis, S. M.: A single parameter representation of hygroscopic growth and cloud condensation nucleus activity, Atmos. Chem. Phys., 7, 1961–1971, https://doi.org/10.5194/acp-7-1961-2007, 2007.

Pöschl, U.: Gas–particle interactions of tropospheric aerosols: Kinetic and thermodynamic perspectives of multiphase chemical reactions, amorphous organic substances, and the activation of cloud condensation nuclei, Atmospheric Research, 101, 562–573, https://doi.org/10.1016/j.atmosres.2010.12.018, 2011.

Reid, J. P., Bertram, A. K., Topping, D. O., Laskin, A., Martin, S. T., Petters, M. D., Pope, F. D., and Rovelli, G.: The viscosity of atmospherically relevant organic particles, Nat. Commun., 9, 956, https://doi.org/10.1038/s41467-018-03027-z, 2018.

Renbaum-Wolff, L., Grayson, J. W., Bateman, A. P., Kuwata, M., Sellier, M., Murray, B. J., Shilling, J. E., Martin, S. T., and Bertram, A. K.: Viscosity of α-pinene secondary organic material and implications for particle growth and reactivity, P. Natl. Acad. Sci. USA, 110, 8014–8019, https://doi.org/10.1073/pnas.1219548110, 2013.

Reyes-Villegas, E., Priestley, M., Ting, Y.-C., Haslett, S., Bannan, T., Le Breton, M., Williams, P. I., Bacak, A., Flynn, M. J., Coe, H., Percival, C., and Allan, J. D.: Simultaneous aerosol mass spectrometry and chemical ionisation mass spectrometry measurements during a biomass burning event in the UK: insights into nitrate chemistry, Atmos. Chem. Phys., 18, 4093–4111, https://doi.org/10.5194/acp-18-4093-2018, 2018.

Saukko, E., Lambe, A. T., Massoli, P., Koop, T., Wright, J. P., Croasdale, D. R., Pedernera, D. A., Onasch, T. B., Laaksonen, A., Davidovits, P., Worsnop, D. R., and Virtanen, A.: Humidity-dependent phase state of SOA particles from biogenic and anthropogenic precursors, Atmos. Chem. Phys., 12, 7517–7529, https://doi.org/10.5194/acp-12-7517-2012, 2012.

Saukko, E., Zorn, S., Kuwata, M., Keskinen, J., and Virtanen, A.: Phase State and Deliquescence Hysteresis of Ammonium-Sulfate-Seeded Secondary Organic Aerosol, Aerosol Sci. Tech., 49, 531–537, https://doi.org/10.1080/02786826.2015.1050085, 2015.

Shao, Y., Wang, Y., Du, M., Voliotis, A., Alfarra, M. R., Turner, S. F., and McFiggans, G.: Characterisation of the Manchester Aerosol Chamber facility, Atmos. Meas. Tech. Discuss. [preprint], https://doi.org/10.5194/amt-2021-147, in review, 2021.

Shilling, J. E., Zawadowicz, M. A., Liu, J., Zaveri, R. A., and Zelenyuk, A.: Photochemical Aging Alters Secondary Organic Aerosol Partitioning Behavior, ACS Earth and Space Chemistry, 3, 2704–2716, https://doi.org/10.1021/acsearthspacechem.9b00248, 2019.

Shiraiwa, M. and Seinfeld, J. H.: Equilibration timescale of atmospheric secondary organic aerosol partitioning, Geophys. Res. Lett., 39, L24801, https://doi.org/10.1029/2012gl054008, 2012.

Shiraiwa, M., Ammann, M., Koop, T., and Pöschl, U.: Gas uptake and chemical aging of semisolid organic aerosol particles, P. Natl. Acad. Sci. USA, 108, 11003–11008, https://doi.org/10.1073/pnas.1103045108, 2011.

Shiraiwa, M., Li, Y., Tsimpidi, A. P., Karydis, V. A., Berkemeier, T., Pandis, S. N., Lelieveld, J., Koop, T., and Pöschl, U.: Global distribution of particle phase state in atmospheric secondary organic aerosols, Nat. Commun., 8, 15002, https://doi.org/10.1038/ncomms15002, 2017.

Slade, J. H., Shiraiwa, M., Arangio, A., Su, H., Pöschl, U., Wang, J., and Knopf, D. A.: Cloud droplet activation through oxidation of organic aerosol influenced by temperature and particle phase state, Geophys. Res. Lett., 44, 1583–1591, https://doi.org/10.1002/2016gl072424, 2017.

Slade, J. H., Ault, A. P., Bui, A. T., Ditto, J. C., Lei, Z., Bondy, A. L., Olson, N. E., Cook, R. D., Desrochers, S. J., Harvey, R. M., Erickson, M. H., Wallace, H. W., Alvarez, S. L., Flynn, J. H., Boor, B. E., Petrucci, G. A., Gentner, D. R., Griffin, R. J., and Shepson, P. B.: Bouncier Particles at Night: Biogenic Secondary Organic Aerosol Chemistry and Sulfate Drive Diel Variations in the Aerosol Phase in a Mixed Forest, Environ. Sci. Technol., 53, 4977–4987, https://doi.org/10.1021/acs.est.8b07319, 2019.

Smith, M. L., Kuwata, M., and Martin, S. T.: Secondary Organic Material Produced by the Dark Ozonolysis of α-Pinene Minimally Affects the Deliquescence and Efflorescence of Ammonium Sulfate, Aerosol Sci. Tech., 45, 244–261, https://doi.org/10.1080/02786826.2010.532178, 2011.

Smith, M. L., Bertram, A. K., and Martin, S. T.: Deliquescence, efflorescence, and phase miscibility of mixed particles of ammonium sulfate and isoprene-derived secondary organic material, Atmos. Chem. Phys., 12, 9613–9628, https://doi.org/10.5194/acp-12-9613-2012, 2012.

Smith, M. L., You, Y., Kuwata, M., Bertram, A. K., and Martin, S. T.: Phase Transitions and Phase Miscibility of Mixed Particles of Ammonium Sulfate, Toluene-Derived Secondary Organic Material, and Water, J. Phys. Chem. A, 117, 8895–8906, https://doi.org/10.1021/jp405095e, 2013.

Song, M., Marcolli, C., Krieger, U. K., Zuend, A., and Peter, T.: Liquid-liquid phase separation in aerosol particles: Dependence on O : C, organic functionalities, and compositional complexity, Geophys. Res. Lett., 39, L19801, https://doi.org/10.1029/2012GL052807, 2012.

Stein, S. W., Turpin, B. J., Cai, X., Huang, P.-F., and McMurry, P. H.: Measurements of relative humidity-dependent bounce and density for atmospheric particles using the DMA-impactor technique, Atmos. Environ., 28, 1739–1746, https://doi.org/10.1016/1352-2310(94)90136-8, 1994.

Tang, I. N. and Munkelwitz, H. R.: Composition and temperature dependence of the deliquescence properties of hygroscopic aerosols, Atmos. Environ. A-Gen., 27, 467–473, https://doi.org/10.1016/0960-1686(93)90204-C, 1993.

Vaden, T. D., Imre, D., Beránek, J., Shrivastava, M., and Zelenyuk, A.: Evaporation kinetics and phase of laboratory and ambient secondary organic aerosol, P. Natl. Acad. Sci. USA, 108, 2190–2195, https://doi.org/10.1073/pnas.1013391108, 2011.

Virtanen, A., Joutsensaari, J., Koop, T., Kannosto, J., Yli-Pirilä, P., Leskinen, J., Mäkelä, J. M., Holopainen, J. K., Pöschl, U., Kulmala, M., Worsnop, D. R., and Laaksonen, A.: An amorphous solid state of biogenic secondary organic aerosol particles, Nature, 467, 824, https://doi.org/10.1038/nature09455, 2010.

You, Y., Smith, M. L., Song, M., Martin, S. T., and Bertram, A. K.: Liquid–liquid phase separation in atmospherically relevant particles consisting of organic species and inorganic salts, Int. Rev. Phys. Chem., 33, 43–77, https://doi.org/10.1080/0144235X.2014.890786, 2014.

Zaveri, R. A., Easter, R. C., Shilling, J. E., and Seinfeld, J. H.: Modeling kinetic partitioning of secondary organic aerosol and size distribution dynamics: representing effects of volatility, phase state, and particle-phase reaction, Atmos. Chem. Phys., 14, 5153–5181, https://doi.org/10.5194/acp-14-5153-2014, 2014.

Zhang, Y., Chen, Y., Lambe, A. T., Olson, N. E., Lei, Z., Craig, R. L., Zhang, Z., Gold, A., Onasch, T. B., Jayne, J. T., Worsnop, D. R., Gaston, C. J., Thornton, J. A., Vizuete, W., Ault, A. P., and Surratt, J. D.: Effect of the Aerosol-Phase State on Secondary Organic Aerosol Formation from the Reactive Uptake of Isoprene-Derived Epoxydiols (IEPOX), Environ. Sci. Tech. Lett., 5, 167–174, https://doi.org/10.1021/acs.estlett.8b00044, 2018.